DISCLAIMER

This report was prepared as an account of work sponsored by an agency of the United States Government. Neither the United States Government nor any agency thereof, nor any of their employees, makes any warranty, express or implied, or assumes any legal liability or responsibility for the accuracy, completeness, or usefulness of any information, apparatus, product, or process disclosed, or represents that its use would not infringe privately owned rights. Reference herein to any specific commercial product, process, or service by trade name, trademark, manufacturer, or otherwise does not necessarily constitute or imply its endorsement, recommendation, or favoring by the United States Government or any agency thereof. The views and opinions of authors expressed herein do not necessarily state or reflect those of the United States Government or any agency thereof. Reference herein to any social initiative (including but not limited to Diversity, Equity, and Inclusion (DEI); Community Benefits Plans (CBP); Justice 40; etc.) is made by the Author independent of any current requirement by the United States Government and does not constitute or imply endorsement, recommendation, or support by the United States Government or any agency thereof.

SANDIA REPORT
SAND2025-11249
Printed September 2025

Sandia National Laboratories

Structural uncertainty assessment for low-Mach wall-resolved large-eddy simulations: Plane Channel and Periodic Hill Use Cases

Stefan P. Domino

Prepared by
Sandia National Laboratories
Albuquerque, New Mexico 87185
Livermore, California 94550

Issued by Sandia National Laboratories, operated for the United States Department of Energy by National Technology & Engineering Solutions of Sandia, LLC.

Available to DOE and DOE contractors from

U.S. Department of Energy
Office of Scientific and Technical Information
P.O. Box 62
Oak Ridge, TN 37831

Telephone: (865) 576-8401
Facsimile: (865) 576-5728
E-Mail: reports@osti.gov
Online ordering: http://www.osti.gov/scitech

Available to the public from

U.S. Department of Commerce
National Technical Information Service
5301 Shawnee Road
Alexandria, VA 22312

Telephone: (800) 553-6847
Facsimile: (703) 605-6900
E-Mail: orders@ntis.gov
Online order: https://classic.ntis.gov/help/order-methods

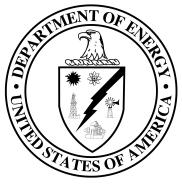

ABSTRACT

A structural uncertainty assessment is provided for a set of wall-resolved large-eddy simulations (WRLES) using a turbulent channel flow (Re_τ 395) and a periodic hill in the turbulent regime (Re^b 2800) validation suite. The standard one-equation subgrid scale turbulent kinetic energy model (k_{sgs}) using both a static and dynamic coefficient approach along with Wall Adapting Local Eddy Viscosity (WALE) are exercised. The k_{sgs} model activated in this study also allows for a correction that supports theoretical turbulent viscosity and total kinetic energy scaling (cubit and quadratic, respectively) in the near-wall regime. Channel and hill results showcase very good agreement between prediction and simulation for the WALE and the dynamic coefficient k_{sgs} model. The study also demonstrates that near-wall damping improves predictivity for the static coefficient k_{sgs} model, while proving an unnecessary additional contribution for the dynamic coefficient k_{sgs} model as near-wall scaling is naturally captured. Overall conclusions are that this suite of WRLES models are well suited for production usage in the Sierra-based low-Mach codes.

This page intentionally left blank.

ACKNOWLEDGEMENT

Funding for this work was provided by the Advanced Simulation and Computing (ASC) program of Sandia National Laboratories. The author would like to thank Stanford researchers including Professor Iaccarino and Mark Benjamin for Inagaki and periodic hill technical discussions during Mark's PhD tenure at Stanford University.

This page intentionally left blank.

CONTENTS

This page intentionally left blank.

LIST OF FIGURES

This page intentionally left blank.

1. INTRODUCTION

While many low-Mach applications of interest to Sandia National Laboratories require a wall-modeled large-eddy simulation (WMLES) formulation (due to the large computational expense associated with resolving a turbulent boundary layer, c.f., the recent fire-engulfed objects subjected to crosswind works of Domino [1] and Domino *et al.* [2]) a robust and theoretically consistent WRLES is of interest to develop, test and deploy to production analysis. The often-exercised standard one-equation static (or constant) coefficient turbulent kinetic energy k_{sgs} model [3] in the WRLES regime generally lacks proper near-wall subgrid scale kinetic energy damping, which drives an overly thick turbulent boundary layer, as the mesh is refined. This general finding has motivated approaches that seek to correct near-wall scaling laws [4]. In this report, we explore alternatives to the static coefficient, one-equation k_{sgs} WRLES approach by the inclusion of damping terms suggested by Inagaki [4] in addition to evaluation of a dynamic coefficient k_{sgs} approach in the WRLES regime. Due to the ubiquity and success of the Wall Adapting Local Eddy Viscosity (WALE) approach [5], evaluation of this model is also of interest and, therefore, included in this WRLES study.

The primary objective of this report is to capture an initial low-Mach validation study in which a plane channel flow and periodic hill use case are used to evaluate a suite of WRLES models to provide credibility statements (i.e., the ability for a simulation to predict quantities of interest (QoIs) such as mean velocity and select Reynolds stresses) along with structural uncertainty assessments (i.e., model-form sensitivity). In Section 2, we overview the variable-density low-Mach turbulent flow WRLES equation set for WALE and k_{sgs}. This section also includes a full description of the additional k_{sgs} source term and turbulent viscosity damping that allows for a theoretically consistent near-wall scaling of turbulent viscosity and turbulent kinetic energy. In Section 3, nuanced code implementations for the Inakaki model [4] are overviewed that have been driven by the lessons learned associated with our study. Channel results (Re_τ 395) of Moser *et al.* [6] are provided in Section 4, while in Section 5 the periodic hill configuration (Re^b 2800 [7]) is presented. Final thoughts and conclusions are captured in Section 6.

This page intentionally left blank.

2. LES MODEL SUITE

The baseline model validation study includes both the wall-adapting local eddy viscosity model [5] and the one-equation turbulent kinetic energy subgrid-scale model, k_{sgs} [3], that has been extended by Inagaki [4] to account for proper near-wall scaling behavior. The dynamic procedure for a localized k_{sgs} model is presented in [8], with implementation details found in Fuego's theory manual [9].

For the LES model overview, we begin with the Favre-filtered momentum equations,

$$\frac{\partial \bar{\rho}\tilde{u}_i}{\partial t} + \frac{\partial \bar{\rho}\tilde{u}_j\tilde{u}_i}{\partial x_j} = \frac{\partial \tilde{\sigma}_{ij}}{\partial x_j} - \frac{\tau_{ij}^{sgs}}{\partial x_j}, \tag{2.1}$$

where the subgrid scale turbulent stress, τ_{ij}^{sgs}, is defined as

$$\tau_{ij}^{sgs} \equiv \bar{\rho}(\widetilde{u_i u_j} - \tilde{u}_i\tilde{u}_j), \tag{2.2}$$

along with the viscous and normal stress, σ_{ij}, given by

$$\sigma_{ij} = 2\mu\tilde{S}_{ij}^{*} - \bar{P}\delta_{ij}. \tag{2.3}$$

Above, the traceless rate-of-strain tensor is,

$$\begin{aligned} \tilde{S}_{ij}^{*} &= \tilde{S}_{ij} - \frac{1}{3}\delta_{ij}\tilde{S}_{kk} \\ &= \tilde{S}_{ij} - \frac{1}{3}\frac{\partial \tilde{u}_k}{\partial x_k}\delta_{ij}, \end{aligned} \tag{2.4}$$

where

$$\tilde{S}_{ij} = \frac{1}{2}\left(\frac{\partial \tilde{u}_i}{\partial x_j} + \frac{\partial \tilde{u}_j}{\partial x_i}\right). \tag{2.5}$$

The deviatoric subgrid stress tensor is,

$$\tau_{ij}^{*sgs} = \tau_{ij}^{sgs} - \frac{1}{3}\delta_{ij}\tau_{kk}^{sgs}, \tag{2.6}$$

where the subgrid turbulent kinetic energy is defined as $\tau_{kk}^{sgs} = 2\bar{\rho}k_{sgs}$. Finally, the modeled turbulent kinetic energy is defined as,

$$k_{sgs} = \frac{1}{2}\left(\widetilde{u_k u_k} - \tilde{u}_k\tilde{u}_k\right). \tag{2.7}$$

The manner in which the subgrid stress tensor that appears in Eq. 2.1 is closed defines the particular LES model in use. Many models used to close the subgrid scale stress are algebraic [10], i.e., do not include extra transport equations, while other approaches include a transport equation. Most baseline approaches define static model constants, while more recent methodologies have allowed for a dynamic approach [11].

2.1. WALE

For the WALE model, an algebraic approach is taken to compute the turbulent viscosity. Moreover, the model-form for the turbulent viscosity is designed such that the near wall turbulent viscosity is a function of the cube of distance from the wall. Away from the wall, the model behaves much like the well-know standard static Smagorinsky model [10]. Given the algebraic form of this model, there are no immediate approaches to augment production of turbulent kinetic energy via baroclinic mechanisms – a possible model requisite for fire use cases.

The description of WALE begins with the turbulent viscosity definition as provided in [5], here shown for completeness using the fully compressible formulation of Han *et al.* [12],

$$\mu_t = \bar{\rho}\left(C_w\Delta\right)^2 \frac{\left(S^d_{ij}S^d_{ij}\right)^{3/2}}{\left(\tilde{S}_{ij}\tilde{S}_{ij}\right)^{5/2} + \left(S^d_{ij}S^d_{ij}\right)^{5/4}}, \tag{2.8}$$

with the constant C_w of 0.325 and a standard filter, Δ related to the dual control volume, $\Delta = V^{\frac{1}{3}}$. The rate of strain, $\tilde{S}_{ij}$, is defined in Eq. 2.5, while S^d_{ij} is,

$$S^d_{ij} = \frac{1}{2}\left(g^2_{ij} + g^2_{ji}\right) - \frac{1}{3}\frac{\partial\tilde{u}_m}{\partial x_l}\frac{\partial\tilde{u}_l}{\partial x_m}\delta_{ij}. \tag{2.9}$$

The velocity gradient squared terms are

$$g^2_{ij} = \frac{\partial\tilde{u}_i}{\partial x_k}\frac{\partial\tilde{u}_k}{\partial x_j} \tag{2.10}$$

and

$$g^2_{ji} = \frac{\partial\tilde{u}_j}{\partial x_k}\frac{\partial\tilde{u}_k}{\partial x_i}. \tag{2.11}$$

We note that the above usage of the dual nodal volume to compute a standard filter yields an averaged length scale over three directions. Sometimes, a minimum edge-length connected to the node is used. However, we have not explored this sensitivity aside from our nonlinear stabilization approach used as a turbulence model where flow-aligned scales are determined by elemental metrics contracted with the velocity field (see Domino *et al.* [13]).

2.2. Standard k_{sgs}

The baseline transport equation for the subgrid kinetic energy activated in this study is given by [3],

$$\frac{\partial \bar{\rho} k_{sgs}}{\partial t} + \frac{\partial \bar{\rho} \tilde{u}_j k_{sgs}}{\partial x_j} + \frac{\partial \tilde{q}_j}{\partial x_j} = \left(P_k - D_k \right), \tag{2.12}$$

where the diffusive flux vector $\tilde{q}_j$ is defined by,

$$\tilde{q}_j = -\left(\frac{\mu}{\sigma_l^k} + \frac{\mu_t}{\sigma_t^k} \right) \frac{\partial k_{sgs}}{\partial x_j}. \tag{2.13}$$

Above, σ_l^k and σ_t^k are laminar and turbulent Schmidt numbers that, for the baseline model, are taken to be 0.9 and 1.0, respectively. The production of subgrid turbulent kinetic energy, P_k, is modeled by,

$$P_k \equiv -\bar{\rho} \widetilde{u_i'' u_j''} \frac{\partial \tilde{u}_i}{\partial x_j}, \tag{2.14}$$

while the dissipation of turbulent kinetic energy, D_k, is given by

$$D_k = \bar{\rho} C_\epsilon \frac{{k_{sgs}}^{\frac{3}{2}}}{\Delta}. \tag{2.15}$$

Finally, the subgrid turbulent eddy viscosity is then provided by

$$\mu_t = \bar{\rho} C_{\mu_\epsilon} \Delta \sqrt{k_{sgs}}. \tag{2.16}$$

Above, the standard model constants for C_ϵ and C_{μ_ϵ} are 0.845 and 0.0856, respectively. For the wall-resolved simulation use case, the subgrid turbulent kinetic energy is zero at the wall while when using a wall function approach, is subjected to a Neumann condition, $\frac{\partial k_{sgs}}{\partial x_j} n_j = 0$, as described in [2]. However, this report does not explore wall-modeled LES for the channel and hill configuration. Recent exploration of so-called exchange-based velocity sampling for WMLES can be found in [2].

2.3. Inagaki k_{sgs} Model

The one-equation form for the Inagaki model is very similar to the baseline model with a few select changes that allow proper scaling of the subgrid scale turbulent kinetic energy near a wall boundary. For more details on the derivation of this model, the reader is referred to Inagaki [4]. In this model, the dissipation rate, D_k, now includes an added dissipation term that is a function of gradients of $\sqrt{k_{sgs}}$, or

$$D_k = \bar{\rho} \epsilon_{sgs} = \bar{\rho} C_\epsilon \frac{{k_{sgs}}^{\frac{3}{2}}}{\Delta} + 2\mu \frac{\partial \sqrt{k_{sgs}}}{\partial x_j} \frac{\partial \sqrt{k_{sgs}}}{\partial x_j}, \tag{2.17}$$

while the turbulent viscosity is modified via a blending coefficient f_μ,

$$\mu_t = \bar{\rho} f_\mu C_{\mu_\epsilon} \Delta \sqrt{k_{sgs}}. \tag{2.18}$$

The functional form for f_μ provided in Inagaki [4] is

$$f_\mu = 1 - exp\left[-\left(\left(\frac{y'_\epsilon}{A_o} \right)^{\frac{2}{3}} \right)^{B_o} \right], \tag{2.19}$$

where the model constants A_o and B_o are 20 and 2, the former of which closely replicates Van Driest scaling while the B_o value of 2 provides the functional form of $f_\mu \propto y^2$ (here, y is the minimum distance to the wall).

The functions y'_ϵ and u'_ϵ are

$$y'_\epsilon = \frac{y u'_\epsilon}{\nu}, \tag{2.20}$$

and

$$u'_\epsilon = \left(\nu \epsilon_{sgs} \right)^{\frac{1}{4}} \sqrt{C_l \frac{y}{\Delta}}. \tag{2.21}$$

The static model constant C_l is specified to be a value of 4. As implied by Eq. 2.17, ϵ_{sgs} is the modified dissipation rate that includes the augmented dissipation by gradients of $\sqrt{k_{sgs}}$,

$$\epsilon_{sgs} = C_\epsilon \frac{{k_{sgs}}^{\frac{3}{2}}}{\Delta} + 2\nu \frac{\partial \sqrt{k_{sgs}}}{\partial x_j} \frac{\partial \sqrt{k_{sgs}}}{\partial x_j}. \tag{2.22}$$

The Inagaki model constants for C_ϵ and C_{μ_ϵ} are now taken to be 0.835 and 0.054, respectively. For the diffusive flux vector, σ_l^k and σ_t^k are specified to be 1.0 and 0.54. We stress that the above equations are a function of the normal distance to the wall, y, thereby requiring a pre-processing step to obtain this quantity.

All simulations presented in this report have been under the uniform-density, incompressible low-Mach form.

3. CODE IMPLEMENTATION

For fast-prototyping, we exercise Nalu [14] – a low-Mach code base that supports both edge- and element-based finite volume methods, and finite element discretization [15]. All baseline turbulence models of interest tested in this paper are implemented in the open domain where arbitrary selection of wall-resolved and wall-modeled boundary conditions are supported in a single simulation. The open-source code is frequently run in the extreme-scale computing regime [16, 17, 18]. An approximate pressure projection scheme [19] with equal-order interpolation is used in this study and has been well-exercised in various generalized unstructured LES studies including coughing and breathing [20, 21], impinging jets [18], and fire use cases [22, 23, 2]. For more simplistic geometries where non-orthogonality is reduced, the edge-based scheme is used, e.g., following our former large-eddy simulation structural uncertainty efforts [24, 25]. Credibility of this numerical approach (either element- or edge-based) in the large-eddy simulation regime on unstructured mesh topologies was established in [26]. At the time of writing this report, WRLES in Fuego (i.e., Sandia's flagship fire environments code [9]) provides the static- and dynamic-based Smagorinsky model, a static coefficeint k_{sgs} model (with or without Inagaki near-wall correction), and a dynamic dynamic k_{sgs} approach. Neither WALE nor a dynamic k_{sgs} model with Inagaki near-wall correction are currently supported in Fuego.

In Nalu and Fuego, the turbulent viscosity is represented as a nodal quantity. To avoid projection of the turbulent viscosity from the element to the nodes, we define a nodal field for the blending constant, f_μ. This blending term is a function of the nodal-based modified dissipation rate, ϵ_{sgs}. To compute this augmented dissipation rate term at a node, the extra term $\frac{\partial\sqrt{k_{sgs}}}{\partial x_j}\frac{\partial\sqrt{k_{sgs}}}{\partial x_j}$ is also required at the nodes of the mesh and is determined by a CVFEM volumetric-based projection,

$$\frac{\partial\sqrt{k_{sgs}}}{\partial x_j} = \frac{\sum_{scv}\frac{\partial\sqrt{k_{sgs}}}{\partial x_j}_{scv}V_{scv}}{\sum_{scv}V_{scv}}. \tag{3.1}$$

This nodal-based quantity can be used for the modified k_{sgs} source term (mass-lumped) and is required for the nodal calculation of ϵ_{sgs} that is used in Eq. 2.19. Our approach removes the requirement to use a standard k_{sgs} projected nodal gradient, $G_j k_{sgs}$, in the calculation of ϵ_{sgs} and, therefore, removes any difficult divide-by-zero approaches that are found in a chain rule-based approach. Should design-order numerics be sought for the k_{sgs} transport equation, the augmented source term can be computed as part of the source term element-based assembly, again using element-based gradient operators as found in Eq. 3.1. Both lumped and consistent source formulations have been tested in Nalu and both performed equally well. In fact, a lumped-mass approach in the element source term assembly mimics a simple nodal loop when the viscosity and k_{sgs} quantities are evaluated at the nodes. In the design-order element-based approach, a nodal f_μ

is required and, thus far, has been nodally lumped, i.e., no consistent mass matrix projection as this alternative approach would require a linear solve for the consistent mass inversion.

4. PLANE CHANNEL

In this section, WRLES results are presented for a standard Re_τ 395 channel and compared to the direct numerical simulation of Moser *et al.* [6]. More details on the mesh and setup can be found in Jofre *et al.* [24]. Adequacy of the mesh spacing was also demonstrated in Jofre *et al.* [24] (maximum y^+ is approximately 0.3) where the WALE model was solely activated. In our current study, the edge-based scheme is activated with linear hexahedral elements and exactly follows the Jofre *et al.* [24] approach, i.e., sub-unity fixed Courant numbers, low-dissipation numerics, and activation of an implicit second-order temporal BDF2 time integrator. Simulations were also run with the baseline CVFEM with very small differences noted (similar to those found in [27]) and are not reported. In Fig. 4-1, the basic landscape of the turbulent channel is shown by providing shadings of velocity and the k_{sgs} field for both time-mean and instantaneous snapshots. The boundary configuration for this case is very simple, requiring a no-slip top and bottom wall in addition to side and streamwise periodic boundaries. A constant body force is applied in the streamwise direction to replicate the required Re_τ 395 value.

For a quantitative perspective, Fig. 4-2 showcases averaged streamwise velocity profiles (u) as a function of vertical distance from the wall (y) using wall units y^+ ($\rho u_\tau y/\mu$) and u^+ (u/u_τ) for the following five LES-based models: WALE, dynamic coefficient k_{sgs} (D-k_{sgs}), dynamic coefficient k_{sgs} with Inagaki's near-wall correction (D-k_{sgs} Inagaki), static coefficient k_{sgs} with Inagaki's near-wall correction (S-k_{sgs} Inagaki), and the static coefficient k_{sgs} model, i.e., without near-wall correction (S-k_{sgs}). In this results set, which includes the DNS data of Moser *et al.* [6], the standard model constants used for the static coefficient k_{sgs} model are $C_{\mu\epsilon}$ = 0.0856 and C_ϵ = 0.845 while for Inagaki, the parameters used are 0.054 and 0.835, respectively. Results show good predictivity for all models with exception of the standard static coefficient k_{sgs} model where an extremely non-physical boundary layer is predicted. Simulations were also carried out using the Inagaki model constants for the non-corrected static coefficient k_{sgs} model (results not included in this report) where the non-physical boundary layer prediction persisted, suggesting that the set of constant changes for the Inagaki model represents a secondary effect. However, the Sierra-based codes Fuego and Nalu allow for user specification of these static coefficients should future studies desire to quantify the precise effect that model constant specifications have on key QoIs.

In Fig. 4-3, the normalized turbulent viscosity as a function of wall unit y^+ profiles are shown for all turbulence models described in this report. Results clearly show non-standard near-wall asymptotic behavior of the static coefficient k_{sgs} model where a first-order functional dependence on y^+ is predicted. The low-Reynolds corrected form of Inagaki (under the static coefficient formulation), WALE, and the dynamic coefficient k_{sgs} model display the expected third-order slope for normalized turbulent viscosity, while the Inagaki dynamic coefficient k_{sgs} model showcases a higher functional dependence on y^+. These results suggest that the additional dynamic procedure

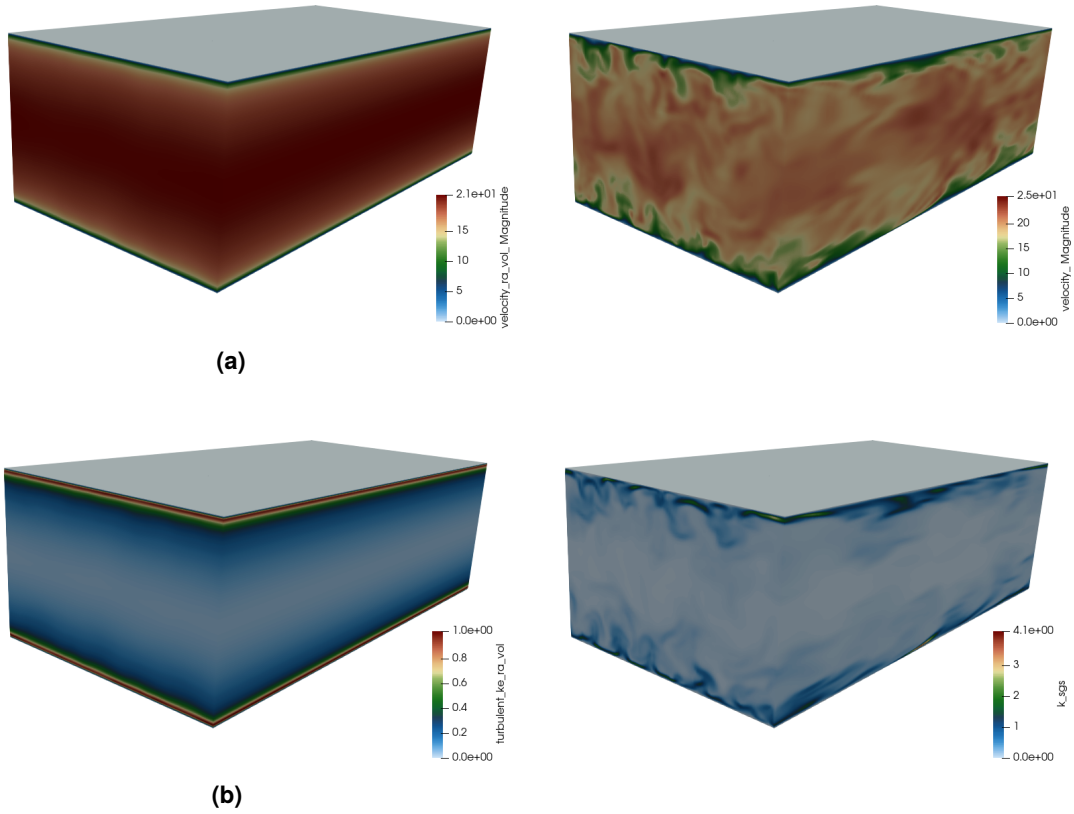

Figure 4-1. Magnitude of velocity (a) and k_{sgs} (b) shadings outlining mean and instantaneous examples in the left and right column, respectively.

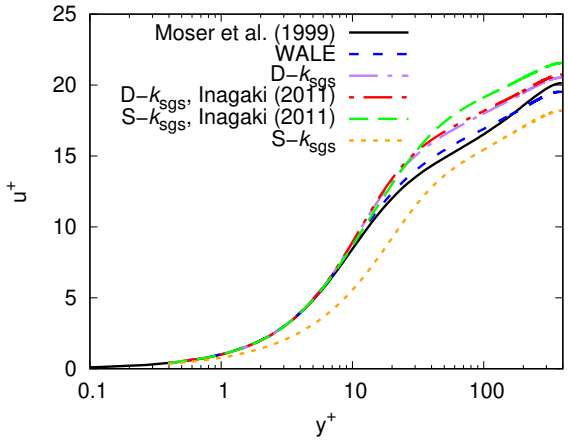

Figure 4-2. Mean streamwise velocity profile (shown in wall units) capturing u^+ as a function of normalized distance to the wall, y^+. In this figure, the DNS data of Moser *et al.* [6] are compared with five turbulence models (model descriptions above).

to the Inagaki model form is not warranted. In general, with the use of a dynamic or near-wall corrected damping, turbulent viscosity decays quickly as the sample points approach the wall.

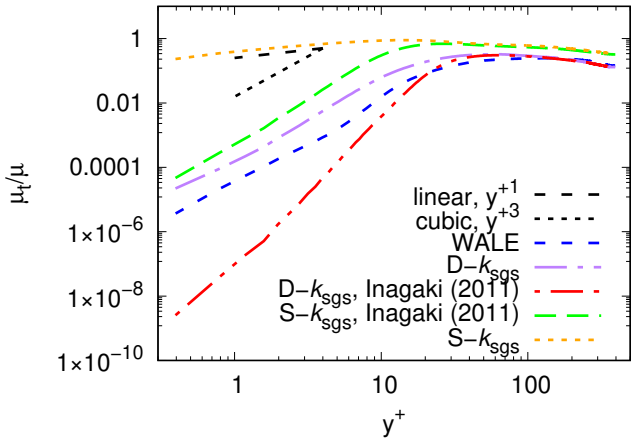

Figure 4-3. Normalized turbulent viscosity for the five turbulence models as described above.

For near-wall behavior of k_{sgs} and total turbulent kinetic energy ($k^{Tot} = k^{Res} + k_{sgs}$) – each quantity has been normalized by u_τ^2 – the reader is referred to Fig. 4-4. For the k_{sgs} plots, WALE is omitted and, thus, its total turbulent kinetic energy captured in panel (b) solely includes the resolved turbulent kinetic energy, $\frac{1}{2}\overline{u_i' u_i'}$. In these particular plots, the resolved turbulent kinetic energy is computed from post-processed LES Reynolds Stress field. Results showcase the errant static coefficient k_{sgs} linear-like behavior of subgrid scale kinetic energy in the near-wall regime, while noting a quadratic-like scaling for the static coefficient Inagaki and dynamic coefficient subgrid scale kinetic energy behavior. This overall scaling is dominated by the tangential fluctuating velocity scaling (linear), and influenced by the faster decaying wall-normal fluctuating velocity component scaling (quadratic) [28]. Finally, it is noted that the Inagaki dynamic coefficient model showcases increased damping as the sample locations approach the wall. All subgrid scale and total turbulent kinetic energy scalings are reasonable, suggesting very good mesh resolution.

For a select description of wall-normal Reynolds stress profiles (u^{RMS}, v^{RMS}, w^{RMS}, and $R_{u'v'}$) as a function of y^+, see Fig. 4-5. WALE and select k_{sgs} results showcase a classic over-prediction of streamwise u^{RMS}, along with under prediction of v^{RMS}, and w^{RMS} that is difficult to avoid, even with an eigenvalue decomposition perturbation and rotation methodology as demonstrated in Jofre *et al.* [24]. However, WALE results appear to be the most predictive over all QoIs, while noting the exceptional prediction of the burst-sweep-controlling $R_{u'v'}$ Reynolds stress.

4.1. General Findings Summary

For the plane channel turbulent flow use case, results suggest that the WALE model provides an improved prediction for the mean velocity profile, while noting a superior prediction for all stresses. The un-corrected static coefficient k_{sgs} model in the vicinity of a wall-resolved surface does not predict the asymptotic behavior of normalized turbulent kinetic energy well (the model demonstrates a first-order dependence on y^+) and falsely predicts a linear dependence of turbulent

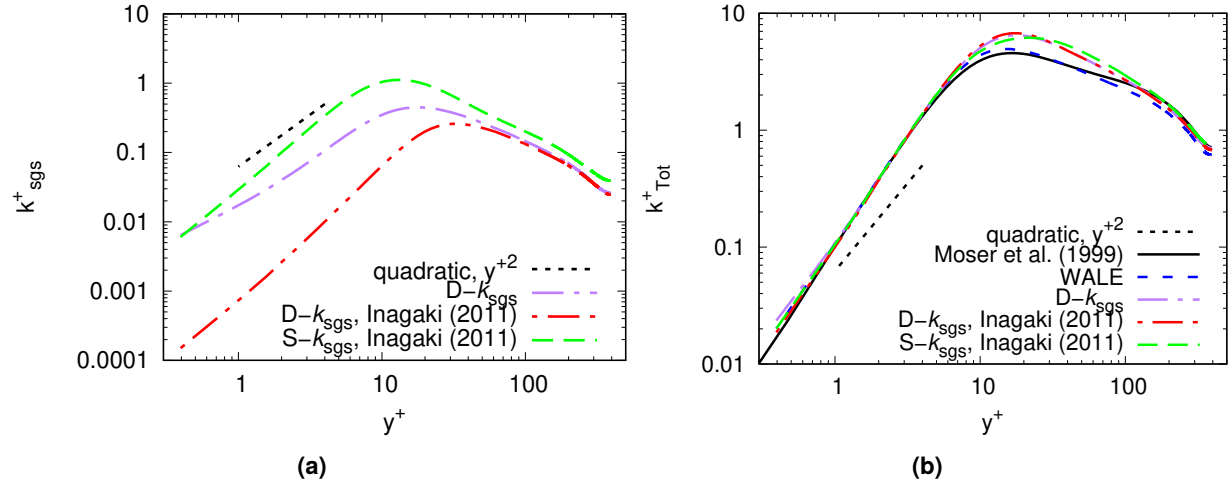

Figure 4-4. Normalized subgrid scale kinetic energy (a) and total turbulent kinetic energy (b) as a function of y^+.

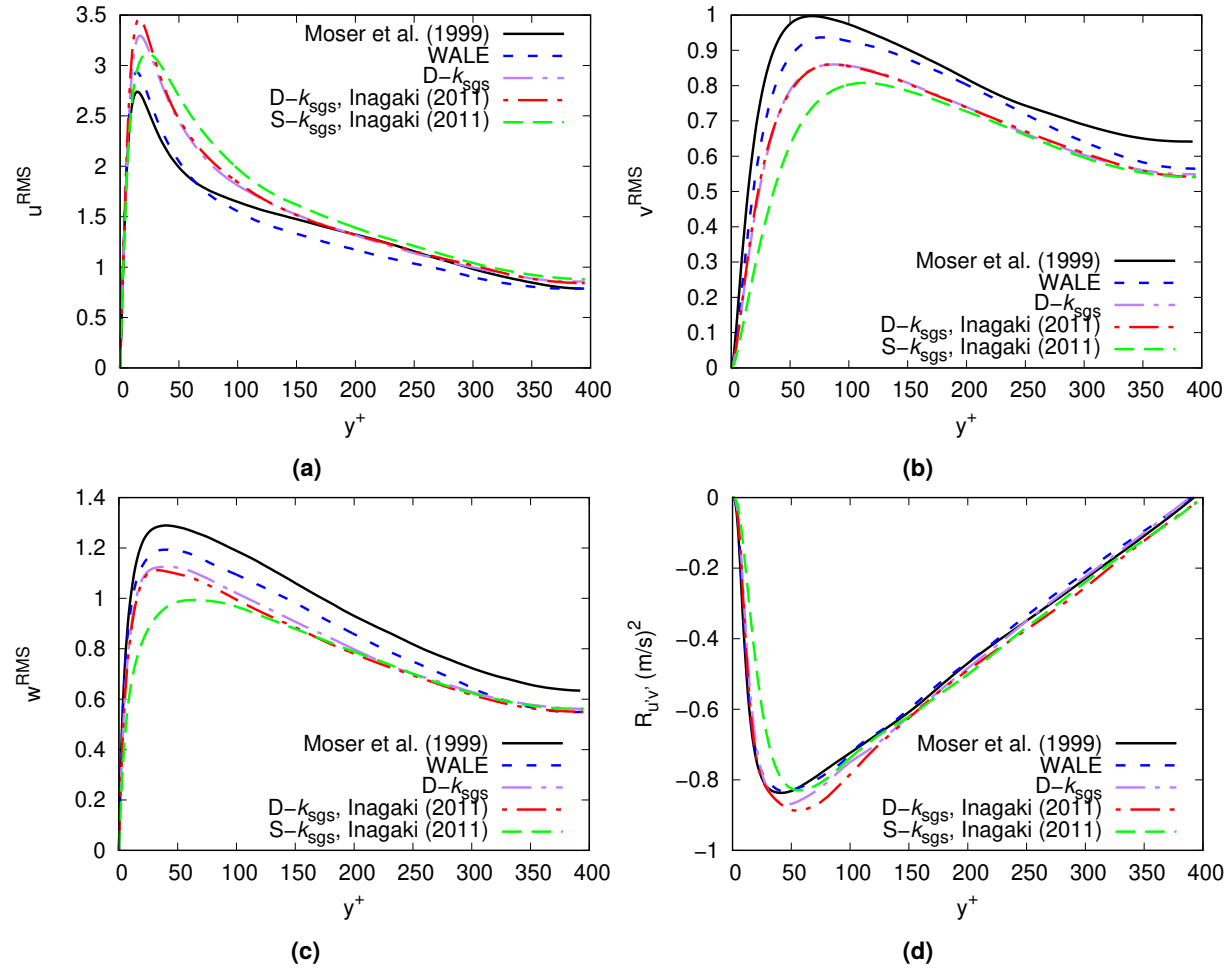

Figure 4-5. Root-mean-square of velocity u (a), v (b), and w (c), in addition to the Reynolds stress, $R_{u'v'}$ (d) for the depicted LES models. Due to already established poor performance of the static coefficient k_{sgs} model, these results have been omitted.

viscosity to y^+. Moreover, the centerline velocity magnitude is also incorrect and is motivated by an unphysical near-wall turbulent viscosity and subgrid scale kinetic energy profile. Conversely, the Inagaki-corrected static coefficient model and non-corrected dynamic coefficient model in the near-wall region both capture a y^+ quadratic functional dependence for normalized turbulent kinetic energy and displays the proper cubic functional dependence on y^+ for the normalized turbulent viscosity. The findings also showcase that the dynamic coefficient procedure for k_{sgs} is sufficient to capture classic near-wall scalings, while noting that the importance to do so is not viewed as critical to the success of a turbulence model [29].

This page intentionally left blank.

5. PERIODIC HILL

The DNS study of Balakumar and Park [7] is now explored in minor detail. For this configuration, the Reynolds number based on the bulk velocity is 2800. Fig. 5-1 outlines the geometry and a WALE result outlining mean and instantaneous velocity shadings. The domain consists of a streamwise, spanwise, and height of dimension 9, 4.5, and 3.035, respectively, with a hill height of unity. The WRLES mesh is approximately one million elements. Again, top and bottom no-slip boundaries are specified along with spanwise and streamwise periodic boundaries. As with the channel flow, a constant streamwise body force is applied. Results indicate that the maximum y^+ is approximately $O(1)$ with this first tested configuration meeting the upper end of acceptable wall normal resolution. A uniform refinement is suggested for complete confidence in mesh-converged results [2]. For this study, the majority of models are run using the edge-based vertex centered scheme, however, a single CVFEM simulation (dynamic coefficient k_{sgs}) is included for a numerical comparison.

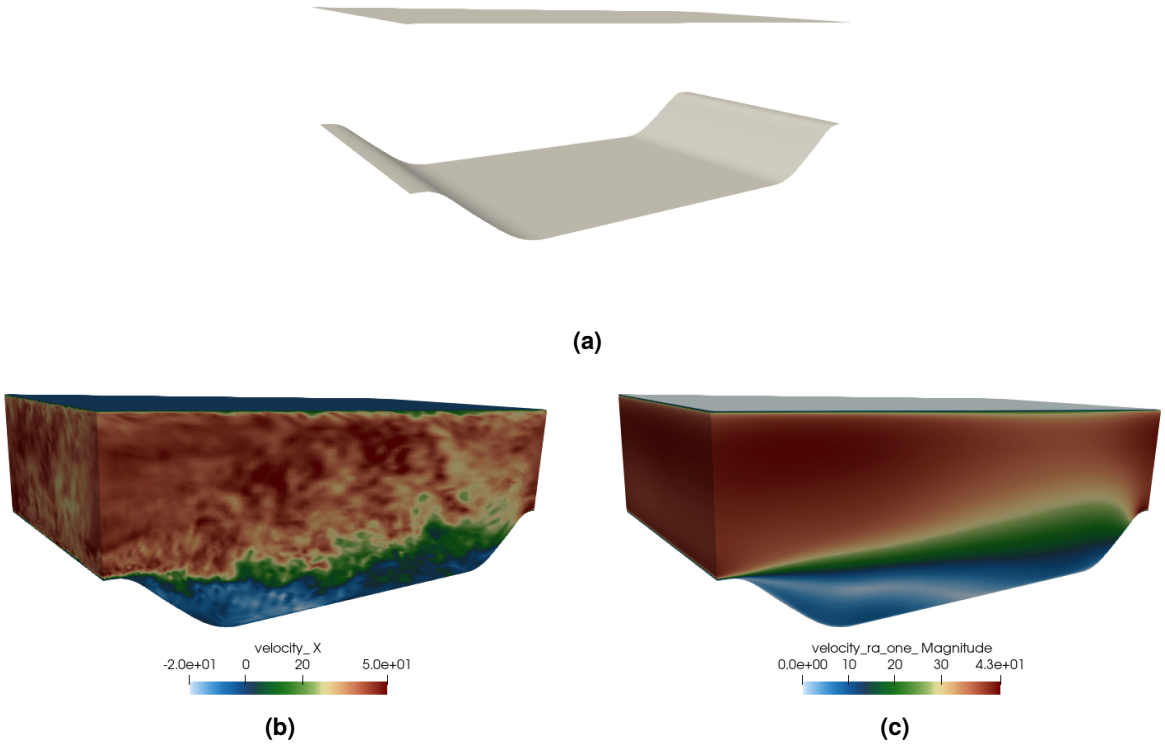

Figure 5-1. Periodic hill geometry (a) and shadings of instantaneous streamwise velocity,(b) and time-mean velocity velocity magnitude, (c).

The extensive DNS results provide a large number of stations within the domain. In this brief write-up, we have showcased the data provided by the author at the "0" (x = 0.0, corresponding to

the left most inlet plane), "4" (x = 1.99125, just past the hill) and "6" (x = 2.9925, within the core recirculation zone). The mean velocity plots, scaled by the inlet predicted bulk velocity, for WALE, dynamic coefficient k_{sgs} (with and without Inagaki's near-wall corrections), static coefficient k_{sgs} with Inagaki's near-wall correction, and the constant coefficient k_{sgs} model without near-wall correction are shown in Fig. 5-2.

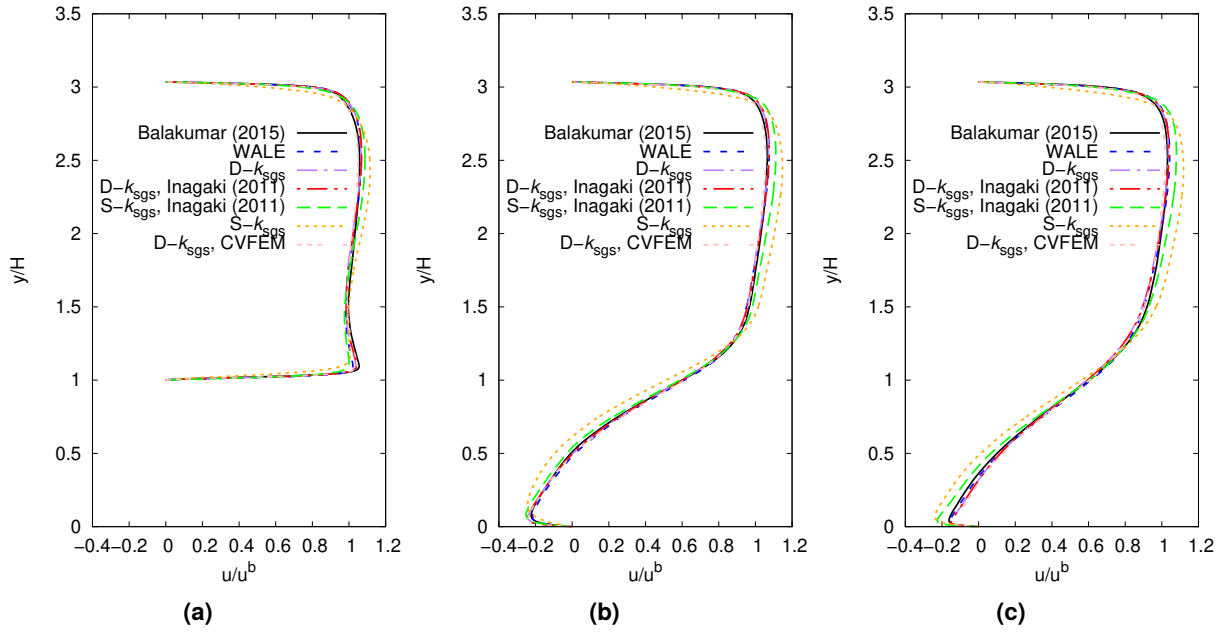

Figure 5-2. Periodic hill mean streamwise velocity normalized by predicted bulk velocity as a function of normalized vertical distance for station(s) 0, 4, and 6 (panels a, b, and c, respectively) of Balakumar and Park [7]. In the above plots, we retain the author's definition of vertical distance, i.e., relative to the bottom hill plane of zero, and normalize distance by the hill height. A single CVFEM result (dynamic coefficient k_{sgs}) represents an additional numerical result.

A consistent theme of improved WALE predictions over the static coefficient k_{sgs} model is noted along with substantial improvement in predictivity when the dynamic k_{sgs} model (non-corrected) is activated. For this case, the static coefficient Inagaki-based approach showcases deviations from the benchmark data set that increase as the stations move downstream. At the top wall, which can be viewed to mimic the channel configuration, we again see a corrupted near-wall velocity profile for the un-damped k_{sgs} model. At station 0 and 4, all models aside from the uncorrected, static coefficient k_{sgs} model predicts mean streamwise velocity profiles extremely well. For the final station, the dynamic procedure applied to the k_{sgs} model out performs the static coefficient k_{sgs} model, with near-wall corrections. Results also showcase very little difference between the edge-based and CVFEM dynamic k_{sgs} results, while noting the typical $2x$ speedup when using the edge-based scheme.

6. CONCLUSIONS

In this report, we have outlined five WRLES models including WALE, dynamic coefficient k_{sgs}, dynamic coefficient k_{sgs} with Inagaki's near-wall correction, static coefficient k_{sgs} with Inagaki's near-wall correction, and the constant coefficient k_{sgs} model without near-wall correction. As highlighted above, the WALE and the dynamic k_{sgs} model each provides the best predictivity at a highly economical cost. The static coefficient Inagaki approach also provides good results, noting that this formulation requires the minimum distance to the wall be post-processed prior to the simulation and adds three new static model constants. The results of plane channel flow also showcase the ability for the dynamic coefficient model to naturally capture near-wall scaling behavior for turbulent viscosity and total turbulent kinetic energy – as found in WALE, by design. However, we find that including both a dynamic procedure along with near-wall Inagaki damping is not justified – both from a theoretical perspective and provided validation that showcases overly damped normalized turbulent viscosity and subgrid scale kinetic energy.

For the more complex periodic hill configuration, both WALE and the dynamic coefficient k_{sgs} again emerge as the best WRLES models based on good agreement with three mean streamwise velocity stations as presented by Balakumar and Park [7]. Virtually no difference between the edge- and element-based numerical approach are noted for the normalized streamwise velocity comparisons using the D-k_{sgs} model. The static coefficient Inagaki model also provides good results suggesting that this is a viable WRLES approach should a dynamic procedure not be implemented.

At the writing of this report, WALE has not been implemented in Fuego, noting that these WRLES findings suggest it can be a powerful production WMLES model. Based on the results found in this report, the dynamic-form of the k_{sgs} Inagaki model need not be implemented/supported in Fuego. Finally, it is suggested to uniformly refine the periodic hill mesh (with surface smoothing) to further investigate the final station mean velocity profiles predictions as a function of mesh spacing. Stresses should also be compared and contrasted for all viable turbulence models.

This page intentionally left blank.

REFERENCES

[1] S. P. Domino. Credibility assessment for WMLES that includes fire-engulfed objects in crosswind. In P. Moin and B. McKeon, editors, *Studying Turbulence Using Numerical Simulation Databases - XIV*, pages 363–372. Stanford Center for Turbulence Research, 2024.

[2] S. P. Domino, S. Scott, and J. Hubbard. Structural uncertainty assessment for fire-engulfed objects in crosswind: Establishing credibility for a multiphysics wall-modeled large-eddy simulation paradigm. *Phys. Rev. Fluids*, 10:054604, May 2025.

[3] A. Yoshizawa. Bridging between eddy-viscosity-type and second-order models using a two-scale dia. *Int. Symp. Turb. Shear Flow*, 3:1–6, 1993.

[4] M. Inagaki. A new wall-damping function for large eddy simulation employing kolmogorov velocity scale. *Int. J. Heat Fluid Flow*, 32(1):26–40, 2011.

[5] F. Nicoud and F. Ducros. Subgrid-scale stress modelling based on the square of the velocity gradient. *Flow Turb. Combust.*, 62:183–200, 1999.

[6] R. D. Moser, J. Kim, and N. N. Mansour. Direct numerical simulation of turbulent channel flow up to $Re_\tau = 590$. *Phys. Fluids*, 11:943–945, 1999.

[7] P. Balakumar and G. I. Park. *DNS/LES Simulations of Separated Flows at High Reynolds Numbers*. Aerospace Sciences Meetings. American Institute of Aeronautics and Astronautics, 2015.

[8] W. Kim and S. Menon. *Application of the localized dynamic subgrid-scale model to turbulent wall-bounded flows*. Aerospace Sciences Meetings. American Institute of Aeronautics and Astronautics, 1997. doi:10.2514/6.1997-210.

[9] Sierra Thermal Fluids Development Team. Sierra low mach module: Fuego theory manual - Version 5.10. Report SAND2022-12438, Sandia National Laboratories, 2022.

[10] J. Smagorinsky. General circulation experiments with the primitive equations. I. The basic experiment. *Mon. Weather Rev.*, 91(3):99–164, 1963.

[11] M. Germano, U. Piomelli, P. Moin, and W. H. Cabot. A dynamic subgrid-scale eddy viscosity model. *Phys. Fluids A Fluid Dyn.*, 3(7):1760–1765, 1991.

[12] H. Qi, X. Li, and C. Yu. A modified wall-adapting local eddy-viscosity model for large-eddy simulation of compressible wall-bounded flow. *Phys. Fluids*, 34(11):116114, 11 2022.

[13] S. P. Domino. Design-order, non-conformal low-Mach fluid algorithms using a hybrid CVFEM/DG approach. *J. Comput. Phys.*, 359:331–351, 2018.

[14] S. P. Domino. Sierra low-Mach Module Nalu: Theory Manual. Technical Report SAND2015-3107W, Sandia National Laboratories SAND Series, Albuquerque, NM, 2014.

[15] S. P. Domino. A comparison between low-order and higher-order low-Mach discretization approaches. In Moin P. and J. Urzay, editors, *Studying Turbulence Using Numerical Simulation Databases - XV*, pages 387–396. Stanford Center for Turbulence Research, 2014.

[16] P. Lin, M. Bettencourt, S. P. Domino, T. Fisher, M. Hoemmen, J. Hu, E. Phipps, A. Prokopenko, S. Rajamanickam, C Siefert, and S. Kennon. Towards extreme-scale simulations for low-Mach fluids with second-generation Trilinos. *Parallel Proccess. Lett.*, 24, 2014.

[17] S. P. Domino and M. Barone. Wind turbine blade wall-resolved large-eddy simulation. Technical Report SAND2016-4085C, Sandia National Laboratories SAND Series, Albuquerque, NM, 2016.

[18] S. P. Domino and E. Wenzel. A direct numerical simulation study for confined non-isothermal jet impingement at moderate nozzle-t o-plate distances: Capturing jet-to-ambient density effects. *Int. J. Heat Mass Transf.*, 211:124168, 2023.

[19] S. P. Domino. Toward verification of formal time accuracy for a family of approximate projection methods using the method of manufactured solutions. In P. Moin and N. Mansour, editors, *Studying Turbulence Using Numerical Simulation Databases - XI*, pages 163–177. Stanford Center for Turbulence Research, 2006.

[20] S. P. Domino, F. Pierce, and J. Hubbard. A multi-physics computational investigation of droplet pathogen transport emanating from synthetic coughs and breathing. *Atomization Spray*, 2021.

[21] S. P. Domino. A case study on pathogen transport, deposition, evaporation and transmission: Linking high-fidelity computational fluid dynamics simulations to probability of infection. *Int. J. Comput. Fluid Dyn.*, pages 1–15, 2021.

[22] S. P. Domino, J. Hewson, R. Knaus, and M. Hansen. Predicting large-scale pool fire dynamics using an unsteady flamelet- and large-eddy simulation-based model suite. *Phys. Fluids*, 33(8):085109, 2021.

[23] S. P. Domino. On the subject of large-scale pool fires and turbulent boundary layer interactions. *Phys. Fluids*, 36(2), 2024.

[24] L. Jofre, S. P. Domino, and G. Iaccarino. A framework for characterizing structural uncertainty in large-eddy simulation closures. *Flow Turb. Combust.*, 99:1–23, 2017.

[25] L. Jofre, S. P. Domino, and G. Iaccarino. Eigensensitivity analysis of subgrid-scale stresses in large-eddy simulation of a turbulent axisymmetric jet. *Int J. Heat Fluid Flow*, 77:314–335, 2019.

[26] S. P. Domino, P. Sakievich, and M. Barone. An assessment of atypical mesh topologies for low-Mach large-eddy simulation. *Comput. Fluids*, 179:655–669, 2019.

[27] S. P. Domino, L. Jofre, and G. Iaccarino. Exploring model-form uncertainties in large-eddy simulation. In P. Moin and J. Urzay, editors, *Studying Turbulence Using Numerical Simulation Databases - XVI*, pages 97–106. Stanford Center for Turbulence Research, 2018.

[28] D. R. Chapman and G. D. Kuhn. The limiting behaviour of turbulence near a wall. *Journal of Fluid Mechanics*, 170:265–292, 1986.

[29] P. Spalart. A Philosophy of Turbulence Modeling, 2025. Accessed on August 8, 2025.

DISTRIBUTION

Email—Internal

Name	Org.	Sandia Email Address
Stefan P. Domino	1541	spdomin@sandia.gov
Technical Library	1911	sanddocs@sandia.gov

This page intentionally left blank.

Sandia National Laboratories is a multimission laboratory managed and operated by National Technology & Engineering Solutions of Sandia LLC, a wholly owned subsidiary of Honeywell International Inc., for the U.S. Department of Energy's National Nuclear Security Administration under contract DE-NA0003525.